Discriminative methods based on sparse representations of pulse oximetry signals for sleep apnea-hypopnea detection

R.E. Rolón[a], L.D. Larrateguy[b], L.E. Di Persia[a], R.D. Spies[c], H.L. Rufiner[a,d]

[a] *Instituto de Investigación en Señales, Sistemas e Inteligencia Computacional, sinc(i), FICH-UNL/CONICET, Santa Fe, Argentina*
[b] *Centro de Medicina Respiratoria de Paraná, Argentina*
[c] *Instituto de Matemática Aplicada del Litoral, IMAL, FIQ-UNL/CONICET, Santa Fe, Argentina*
[d] *Laboratorio de Cibernética, Fac. de Ing., Univ. Nacional de Entre Ríos, Argentina*

Abstract

The obstructive sleep apnea-hypopnea (OSAH) syndrome is a very common and generally undiagnosed sleep disorder. It is caused by repeated events of partial or total obstruction of the upper airway while sleeping. This work introduces two novel approaches called most dicriminative activation selection (MDAS) and most discriminative column selection (MDCS) for the detection of apnea-hypopnea events using only pulse oximetry signals. These approaches use discriminative information of sparse representations of the signals to detect apnea-hypopnea events. Complete (CD) and overcomplete (OD) dictionaries, and three different strategies (FULL sparse representation, MDAS, and MDCS), are considered. Thus, six methods (FULL-OD, MDAS-OD, MDCS-OD, FULL-CD, MDAS-CD, and MDCS-CD) emerge. It is shown that MDCS-OD outperforms all the others methods. A receiver operating characteristic (ROC) curve analysis of this method shows an area under the curve of 0.937 and diagnostic sensitivity and specificity percentages of 85.65 and 85.92, respectively. This shows that sparse representations of pulse oximetry signals is a very valuable tool for estimating apnea-hypopnea indices. The implementation of the MDCS-OD method could be embedded into the oximeter so as to be used by primary attention clinical physicians in the search and detection of patients suspected of suffering from OSAH.

Keywords: Sleep apnea-hypopnea syndrome, Sparse representations, Dictionary learning, Neural networks

1. Introduction

In the year 2014 the American academy of sleep medicine (AASM) released the third edition of the international classification of sleep disorders [1]. One of the most common sleep disorders is the obstructive sleep apnea-hypopnea (OSAH) syndrome, which is caused by repeated events of partial (hypopnea) or total (apnea) obstruction of the upper airway while sleeping. To establish the degree of severity of the syndrome, the apnea-hypopnea index (AHI) is created. The AHI represents the number of apnea-hypopnea events per hour of sleep. The OSAH is classified as normal, mild, moderate or severe if belongs to the interval $[0, 5)$, $[5, 15)$, $[15, 30)$, or $[30, \infty)$, respectively.

Nowadays, the gold standard test for diagnosing sleep disorders is a polysomnography (PSG) in a sleep medical center. However the accessibility to this type of study is usually very limited as well as costly in terms of both time and money. A complete PSG consists of simultaneous measurement of several physiological signals such as electrical activity of the brain along the scalp, electrical activity of the heart using electrodes placed on the body's surface, electrical activity produced by skeletal muscles, respiratory effort, airflow and blood oxygen saturation (SaO_2) signals, among others. Mainly due to its ease of acquisition, we are particularly interested in the latter. In a typical PSG study, after a normal period of sleep the recorded signals are provided to medical experts. Due to its complexity, different alternatives to PSG have been developed. One of the most popular alternatives to PSG is the so called home respiratory polygraphy [2]. Although some studies have shown that there is a very high correlation between AHIs generated by polygraphy and PSG studies and polygraphy requires no neurophysiological signals [3], it still needs several others physiological signals, whose acquisition affects the normal sleeping of the persons. It is therefore highly desirable to develop a reliable system which makes use of as few as possible physiological signals. Since pulse oximetry is a well know, quite cheap and non-invasive technique, it has become a very valuable alternative to detect persons suspected of suffering from OSAH [4]. A recent work has shown that statistical analysis and feature extraction methods applied to pulse oximetry signals provide satisfactory diagnostic performance in detecting severe OSAH patients [5]. Cessation of breathing associated with apnea-hypopnea events are always accompanied by a drop in the oxygen saturation level. It is appropri-

ate to mention however that this drop level can be very small and impossible to detect by a human observer, reason for which advanced signal processing techniques such as artificial intelligence methods could provide a very valuable alternative. A decrease in blood oxygen saturation usually produces changes in the pulse oximetry record corresponding to intermittent hypoxemia. The intermittent hypoxemia, with hypoxemia-reoxygenation cycles, very often indicates OSAH syndrome.

Pulse oximetry, besides providing information about blood oxygen saturation during sleeping, is used for computing some parameters which quantify desaturation levels in the SaO_2 signal. The seek of patients suspected of suffering from OSAH can be addressed by means of two different approaches. A *global* approach consists of obtaining general characteristics of the SaO_2 signal, such as its mean, variance and entropy values, among others with the only objective of classifying a person as healthy or sick without taking into consideration the degree of severity of the illness. In this work a *local* approach, which allows a more thorough analysis of the SaO_2 signal, is taken. This approach consists of detecting the apnea-hypopnea events from sparse representations of segments of SaO_2 signals using a neural network classifier. The local approach was previously used for estimating three parameters denoted by ODI4, ODI3, and ODI2, which are defined as the number of times per hour of sleep that the SaO_2 signal decreases below 4%, 3%, and 2% of a baseline level, respectively. It is timely to point out, however that although the concept of "baseline level" is very intuitive, it is not uniquely defined and different criteria and definitions have been adopted by different authors [6, 7].

In the last fifteen years, a wide variety of machine learning algorithms were used for detecting several health disorders [8]. Implementations of these algorithms were applied to detect particular sleep disorders and different signal processing techniques originating new methods based on non-linear systems, higher-order statistics, spectral analysis, including independent component analysis (ICA) [9, 10, 11]. Moreover pattern recognition algorithms based on artificial neural network (ANN) were successfully applied to assist OSAH diagnosis and classification [12]. Nowadays, a powerful method based on sparse representations of signals finds the solution corresponding to the most compact representation by means of a linear combination of atoms in a dictionary [13, 14]. It was found that this approach, when applied to biological sensory systems, results in internal representations having properties similar to the real ones, in particular similar to those found in the primary

auditive or visual cortex of the mammals [15, 16]. Some of the advantages of the sparse representations are: super resolution, robustness to noise and dimension reduction, among others. The sparse representations of signals provide new grounds for treating both the signal modeling and the representation problems. The dictionary is learned for the purpose of obtaining the best representation of a given set of signals, although the atoms involved in such representation are not necessarily the atoms which capture discriminative information. It is therefore clear that if the SaO_2 signal is to be used as the only input for detection of apnea-hypopnea events, advanced signal processing algorithms capable of extracting discriminative information from sparse representations of signals will be needed.

In this work we present two novel methods called "most discriminative activation selection" (MDAS) and "most discriminative column selection" (MDCS) based on sparse representations of SaO_2 signals. A preliminary related approach of this work has been reported in [17]. The methods MDAS and MDCS involve finding an optimal subset of most discriminative atoms and the corresponding configuration of a multilayer perceptron (MLP) neural network classifier for detecting apnea-hypopnea events from sparse representations of segments of SaO_2 signals. The apnea-hypopnea events were appropriately labeled by medical experts, who have been carefully analyzed the complete PSG. Our methods allow for a significant reduction in the dimension of the inputs to the MLP neural network, preserving the most important characteristics of the SaO_2 signal.

This article is organized as follows: in Section 2 the materials and methods used for obtaining sparse representations of SaO_2 signals are explained. In Section 3 the results are described and the discussion is finally included in Section 4.

2. Materials and Methods

A sparse representation problem can be divided into two separate subproblems: a *learning* problem and an *inference* problem. The first one, which is quite often more complex, consists of finding an "optimal" dictionary Φ to represent a given set of signals $\{\mathbf{x}_i\}$. A dictionary Φ is called complete (CD) or overcomplete (OD) depending on the number of basic waveforms be equal or greater, respectively than the signal's space dimension. The second problem consists of selecting a set of representation vectors $\{\mathbf{a}_i\}$ satisfying a given sparsity constraint. The MDAS and MDCS methods involve finding

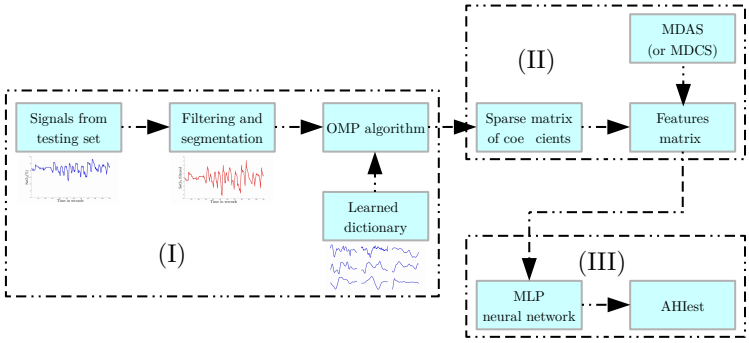

Figure 1: A simplified block diagram of the classification process.

a set of discriminative coefficients (feature vector) to be used as inputs of a MLP neural network [18]. In order to achieve this objective all possible number of inputs (F) and a large number of neurons in its hidden layer (NHL) are tested. Finally the optimal configuration is obtained by choosing the F and NHL values resulting in the best performance.

Figure 1 shows a simplified block diagram of the proposed system. In the first block (I) the signals are filtered and segmented by making use of wavelet filters [19] and segmentation techniques (as described in Subsection 2.1), respectively. The processes for obtaining sparse representations of the signals are presented by a previously learned dictionary and orthogonal matching pursuit (OMP) algorithm. The second block (II) shows the feature extraction stage by using the MDAS (or MDCS) method (see details in Subsection 2.4). In the last block (III), the estimated AHI ($\mathrm{AHI}_{\mathrm{est}}$) value is obtained by post-processing a previously trained MLP neural network output which produces the apnea-hypopnea event detection (see details in Sections 2.3 and 3).

We consider two types of dictionaries (complete and overcomplete) and three different methods (use of the FULL sparse representation, MDAS and MDCS). Thus, six methodologies emerged, which we call FULL-OD, MDAS-OD, MDCS-OD, FULL-CD, MDAS-CD, and MDCS-CD. Thus, for instance, the FULL-OD method makes use of an overcomplete dictionary Φ_{OD} and the whole representation vector $\mathbf{a}_i$ as input of the MLP neural network classifier, while the MDAS-OD method uses the dictionary Φ_{OD} and a selected set of features extracted from $\mathbf{a}_i$ by applying the MDAS method.

2.1. Filtering and segmentation

The set of biomedical signals used in this article was obtained from the sleep heart health study (SHHS) dataset [20, 21]. This dataset comprises valuable material about detailed PSGs which were properly obtained to explore correlations between sleep disorders and cardiovascular diseases. The complete dataset includes 995 studies, each of them containing several biomedical signals such as electrical activity of the brain, electrical activity of the heart, nasal airflow, SaO_2, among others. Annotations of sleep stages, arousals and apnea-hypopnea events are also added. For our work, only the SaO_2 signal and its corresponding apnea-hypopnea labels are considered.

The SaO_2 signals are usually highly degraded by patient movements, baseline wander, disconnections and the limited resolution of the pulse oximeter, among others factors. When a disconnection occurs, the values during the time interval where the sensor signal is invalid are linearly interpolated. A wavelet processing technique proposed in [19] is chosen for denoising the signals. The signals are also sampled at 1Hz and the denoising process is carried out by discarding the approximation coefficients, at level 8, as well as the first three detail coefficients of the discrete dyadic wavelet transform with mother wavelet Daubechies 2. The application of this process has the effect of a band-pass filter where the baseline wander and both the low frequency noise and the high frequency noise as well as the quantization noise are eliminated. Figure 2 shows a portion of the airflow signal (top) as well as the original raw pulse oximetry signal (middle) and the wavelet-filtered pulse oximetry signal (bottom). The corresponding labels of apnea-hypopnea events (dash lines) are also included. By observing both the airflow and the raw pulse oximetry signals, it can be seen that there is generally a causal relation between an apnea-hypopnea event and the oxygen desaturation in the pulse oximetry signal. However, the time interval between the blockage of nasal airflow and the start of the oxygen desaturation is highly variable. Although, as previously mentioned an apnea-hypopnea event is not always accompanied with "noticeable" oxygen desaturations (which are used by medical experts to detect and label the apnea-hypopnea events), artificial intelligent algorithms can detect slight changes in the pulse oximetry signal. Note that the time duration of each desaturation, which is associated to an apnea-hypopnea event, is also variable. Figure 2 also shows the effect of the wavelet-filter in avoiding "disconnections" in the pulse oximetry signal. In what follows, by the "SaO_2 signal", we will always mean the denoised one.

In order to apply the sparse representation technique, an appropriate

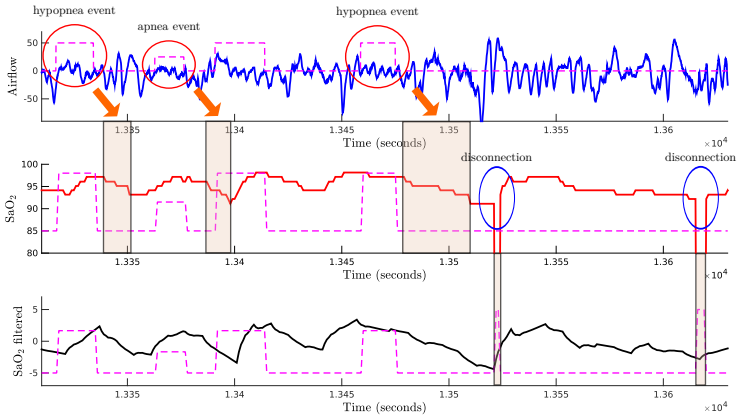

Figure 2: A portion of airflow and pulse oximetry signals. Original raw airflow and pulse oximetry signals (top and middle) and its wavelet-filtered version (bottom). Dashed lines represent labels of apnea-hypopnea events introduced by the medical expert.

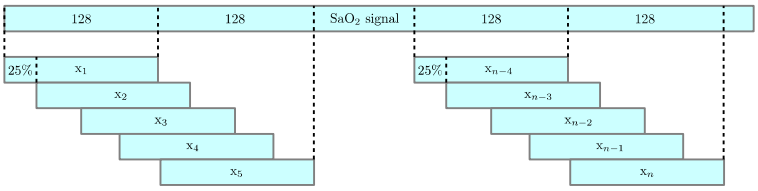

Figure 3: Schematic representation of SaO_2 signal segmentation.

segmentation of the signals is required. For this reason, segments of length $N = 128$ (corresponding to 128 seconds) with a 75% overlapping between two consecutive segments are taken. In this process, the time intervals where a disconnection occurs are not taken into account. The segmentation process is depicted in Figure 3. The segments of pulse oximetry signals are simultaneously arranged as column vectors $\mathbf{x}_i \in \mathbb{R}^N$ and labeled with ones and minus ones, where a one is associated to an apnea-hypopnea event, and a minus one to the lack of it, respectively. Finally a signal matrix X is built by stacking side-by-side the column vectors $\mathbf{x}_i$, i.e. the signal matrix is defined as $\mathrm{X} \doteq [\mathbf{x}_1\ \mathbf{x}_2\ \mathbf{x}_3\ \cdots\ \mathbf{x}_n]$, where n represents the total number of segments.

2.2. Sparse representations

The problem of obtaining the sparse representation of a signal $\mathbf{x}_i$ in terms of a given overcomplete dictionary Φ can be described as follows: Given both a matrix $\Phi \in \mathbb{R}^{N \times M}$ (with $M \geq N$) formed by M columns ϕ_j (called atoms

of the dictionary) and a signal $\mathbf{x}_i \in \mathbb{R}^N$, the sparse representation problem can be written as $\mathbf{x}_i = \Phi \mathbf{a}_{\mathrm{SR}(i)}$; where

$$\mathbf{a}_{\mathrm{SR}(i)} \;=\; \underset{\mathbf{a}_i}{\operatorname{argmin}} \, ||\mathbf{a}_i||_0 \text{ subject to } \Phi \mathbf{a}_i = \mathbf{x}_i, \tag{1}$$

where the operator $||\cdot||_0$ denotes the zero-norm.

The term "basis" is often replaced by "dictionary" because the atom-by-atom linear independence is not necessary needed, and many times the number of atoms is greater than the dimension of the signals. In that case, i.e. $M > N$, or more generally when the atoms do not form a basis, then the representation of a given signal may not be unique and therefore a good enough constraint is required to choice only one of them. In our case, sparsity (a criterion for selecting a representation using the least number of atoms) is used, although many other available criteria can be taken into account.

By considering the representation given by $\mathbf{x}_i = \Phi \mathbf{a}_i$. It is important to point out that although the synthesis of the signals is linear, the opposite operation (obtain $\mathbf{a}_i$ in terms of $\mathbf{x}_i$ and Φ) can be non-linear.

In practical applications not just one but a given set of signals is normally obtained. In this case the problem of sparse representation of such signals becomes very difficult because the build up of the dictionary is part of the problem. Naturally the dictionary could be constructed by staking side-by-side the whole signals. Although the sparse representation problem will be optimal, this kind of solution is highly undesired because of its huge size and long redundancy. Thus it is very appropriate to use a method which learn an optimal dictionary, in certain sense, from de signals in the given dataset. To achieve this objective a statistical approach called noise overcomplete ICA (NOCICA) [13, 22, 23] was taken. Equations (2) and (3) describe iterative rules for updating both the dictionary Φ and the representation vector $\mathbf{a}$ by means of this method:

$$\Delta\Phi = \eta \Lambda_\epsilon ((\mathbf{x} - \Phi \mathbf{a}_{\mathrm{MAP}}) \mathbf{a}_{\mathrm{MAP}}^T - \Phi H^{-1}), \tag{2}$$

where $\eta \in (0, 1)$ is the so called "learning coefficient", Λ_ϵ is the noise covariance matrix, $\mathbf{a}_{\mathrm{MAP}}$ is the maximum-a-posteriori (MAP) estimator of $\mathbf{a}$ and H is minus the Hessian of the log-posterior evaluated at $\mathbf{a}_{\mathrm{MAP}}$, and

$$\Delta\mathbf{a} = \Phi^T \Lambda_\epsilon (\mathbf{x} - \Phi \mathbf{a}) - \boldsymbol{\rho}^T |\mathbf{a}|, \tag{3}$$

where $\boldsymbol{\rho} = (\rho_1 \;\; \rho_2 \;\; \cdots \;\; \rho_n)^T$ corresponds to a proposed a Laplacian a-priori distribution $\pi(a_j) \propto \exp(\rho_j |a_j|)$ and $\rho_j < 0$.

2.3. MLP neural network

The MLP is a special type of neural networks which consist of input units (input layer), at least one hidden layer and an output layer [18]. Both the hidden an the output layers are composed of computation units (neurons). The inputs, sometimes called feature vector, are processed layer-by-layer moving forward through the network. The output of a neuron is given by the application of an activation function (linear or non-linear) to the weighted sum of the inputs plus a bias term. In general the output of a neuron y_j is given by Equation (4).

$$y_j = f(\sum_{i=1}^{d} \omega_{ji} x_i + \omega_{j0}) = f(\sum_{i=0}^{d} \omega_{ji} x_i), \tag{4}$$

where the activation function (sometimes called transfer function) is denoted by $f(\cdot)$, and the weights connecting the i-th input to the j-th neuron for a given layer is represented by ω_{ji}.

2.4. Detection of discriminative atoms

As already explained, the problem of sparse representations of a signal consist essentially in approximating such a signal by a linear combination of only a few atoms in a given dictionary. In applications whose final objective is signal classification we are not much interested in the accuracy of such a representation but rather in its discriminative power, that is in its ability to distinguish between the different classes. With this in mind, in this work we introduce an atom selection process by means of discriminative information. Roughly speaking, when an atom has a high activation frequency for one of the classes (but not for the others), then this atom is classified as containing significant "discriminative" information. The MDAS and MDCS methods are explained below.

The MDAS method: let Φ be a given dictionary, $\mathrm{X}_{\mathrm{train}}$ and $\mathrm{X}_{\mathrm{val}}$ training and validation signal matrices, respectively (built as explained in Subsection 2.1), $\mathrm{T}_{\mathrm{train}}$ and $\mathrm{T}_{\mathrm{val}}$ training and validation target vectors, respectively, and p_0 the sparsity level. We describe now the building steps of the MDAS method together with the corresponding lines in its implementation algorithm (Algorithm 1). First, each representation vector $\mathbf{a}_{\mathrm{SR(i)}}$ is obtained by applying a greedy pursuit algorithm called OMP [24] (line 2). Then a coefficient matrix A is assembled by stacking side-by-side the vectors $\mathbf{a}_{\mathrm{SR(i)}}$ (line 3). After that, the atom activation frequencies η_κ^j are obtained for each one of the atoms $\boldsymbol{\phi}_j$ and each one of the classes $\kappa = 1$ and $\kappa = 2$ (line

5). Here, η_κ^j represents the number of times that the atom $\boldsymbol{\phi}_j$ was used to represent segments belonging to the class κ and τ_κ represents the column indices corresponding to class κ. The proposed discriminative approach begins by computing the absolute difference between the activation frequencies, i.e. $\mathrm{D}(j) = |\eta_1^j - \eta_2^j|$ (line 6). Clearly $\mathrm{D}(j)$ will be large if the j^{th}-atom is much more active in one class than in the other. Otherwise, if the j^{th}-atom has similar activation frequencies in both classes then $\mathrm{D}(j)$ is close to zero. After that the vector D is redefined by rearranging its elements in decreasing order and saving the corresponding vector of indices Ind (lines 8 and 9). Next the MLP neural network is trained by varying the feature vector size and the number of neurons located in the hidden layer (lines 10 to 19). The features taken as input of the MLP neural network are those corresponding to the most discriminative atoms of Φ according to D ($\mathrm{F}_{\mathrm{MDAS}}$ for training and $\mathrm{F}_{\mathrm{val}}$ for validation). Once the MLP neural network training stage is finished, an optimal configuration of the MLP neural network is obtained (line 20). An schematic representation of the coefficient selection process is depicted in Figure 4. Figure 5 shows, in decreasing order, the absolute difference of activation frequencies of the atoms corresponding to a dictionary which was learned using segments of signals belonging to class 1. By observing this figure it is reasonable to conclude that a large percentage of the discriminative information can be captured by the first 40 or 50 atoms. Figure 6 shows the waveforms of some atoms in three different regions of the curve shown in Figure 5. In particular the first row in Figure 6 shows the waveforms of the first three most discriminative atoms while rows 2 and 3 present the waveforms corresponding to atoms in the middle and low discrimination ranges, respectively. It is very interesting to see that the three first most discriminative atoms present waveforms which are clearly associated with desaturations in the SaO_2 signals.

The MDCS method: this method (whose implementation is described by Algorithm 2) is similar to the previous one except for the stage 2 that we describe next. Once the vector D is rearranged, a new sub-dictionary Φ_{new} is built (line 4) and consequently the feature vector $\mathbf{f}_i$ is obtained by applying the OMP algorithm (line 5). Finally each feature vector $\mathbf{f}_i$ is assigned to be the input of the MLP neural network (line 7).

At the training stage most of the computational cost (about 80%) is due to dictionary learning. The remaining cost corresponds to the inference of the coefficients and the MLP neural network training. At the testing stage the computational cost is significantly reduced (at about 30% of the training

Algorithm 1 MDAS algorithm

procedure MDAS($\Phi, \mathrm{X}_{\mathrm{train}}, \mathrm{X}_{\mathrm{val}}, \mathrm{T}_{\mathrm{train}}, \mathrm{T}_{\mathrm{val}}, p_0$)
stage 1:
  $\mathbf{a}_{\mathrm{SR(i)}} \leftarrow \underset{\|\mathbf{a}_i\|}{\operatorname{argmin}} \|\mathbf{x}_i - \Phi\mathbf{a}_i\|_2^2$
    subject to $\|\mathbf{a}_i\|_0 \leq p_0,\ \forall \mathbf{x}_i \in \mathrm{X}_{\mathrm{train}}$
  $\mathrm{A} \leftarrow [\mathbf{a}_{\mathrm{SR}(1)}\ \mathbf{a}_{\mathrm{SR}(2)}\ \mathbf{a}_{\mathrm{SR}(3)}\ \cdots\ \mathbf{a}_{\mathrm{SR}(n)}]$
  for $j \leftarrow 1, M$ **do**
    $\eta_\kappa^j \leftarrow \|\mathrm{A}(j, \tau_\kappa)\|_0$
    $\mathrm{D}(j) \leftarrow |\eta_1^j - \eta_2^j|$
  end for
  $\mathrm{D} \leftarrow [\mathrm{d}_{\gamma(1)}\ \mathrm{d}_{\gamma(2)}\ \mathrm{d}_{\gamma(3)}\ \cdots\ \mathrm{d}_{\gamma(M)}]$
  $\mathrm{Ind} \leftarrow [\gamma(1)\ \gamma(2)\ \gamma(3)\ \cdots\ \gamma(M)]$
stage 2:
  for $m \leftarrow 1, M$ **do**
    $\mathrm{Ind}_{\mathrm{new}} \leftarrow [\mathrm{Ind}(1)\ \cdots\ \mathrm{Ind}(m)]$
    for $h \leftarrow 1, N$ **do**
      $\mathbf{f}_i \leftarrow \mathbf{a}_{\mathrm{SR(i)}}\,(\mathrm{Ind}_{\mathrm{new}})$
      $\mathrm{F}_{\mathrm{MDAS}} \leftarrow [\mathbf{f}_1\ \mathbf{f}_2\ \mathbf{f}_3\ \cdots\ \mathbf{f}_n]$
      $\mathrm{NHL} \leftarrow h$
      net $\leftarrow$TRAIN($\mathrm{F}_{\mathrm{MDAS}}, \mathrm{T}_{\mathrm{train}}, \mathrm{NHL}$)
      $\mathrm{PM}(n, m) \leftarrow$ VALID(net, $\mathrm{F}_{\mathrm{val}}, \mathrm{T}_{\mathrm{val}}$)
    end for
  end for
stage 3:
  $[\mathrm{F}_{\mathrm{op}}, \mathrm{NHL}_{\mathrm{op}}] \leftarrow \underset{\mathrm{F,NHL}}{\operatorname{argmax}}\ \mathrm{PM}$
  return $\mathrm{F}_{\mathrm{op}}, \mathrm{NHL}_{\mathrm{op}}$
end procedure

Algorithm 2 MDCS algorithm

procedure MDCS($\Phi, \mathrm{X}_{\mathrm{train}}, \mathrm{X}_{\mathrm{val}}, \mathrm{T}_{\mathrm{train}}, \mathrm{T}_{\mathrm{val}}, p_0$)
stage 1: same as MDAS algorithm
stage 2:
  for $m \leftarrow 1, M$ **do**
    $\mathrm{Ind}_{\mathrm{new}} \leftarrow [\mathrm{Ind}(1) \ \cdots \ \mathrm{Ind}(m)]$
    $\Phi_{\mathrm{new}} \leftarrow \Phi(:, \mathrm{Ind}_{\mathrm{new}})$
    $\mathbf{f}_i \leftarrow \underset{\|\mathbf{a}_i\|}{\operatorname{argmin}} \|\mathbf{x}_i - \Phi_{\mathrm{new}}\mathbf{a}_i\|_2^2$
      subject to $\|\mathbf{a}_i\|_0 \leq p_0$
    for $h \leftarrow 1, N$ **do**
      $\mathrm{F}_{\mathrm{MDCS}} \leftarrow [\mathbf{f}_1 \ \mathbf{f}_2 \ \mathbf{f}_3 \ \cdots \ \mathbf{f}_n]$
      $\mathrm{NHL} \leftarrow h$
      $\mathrm{net} \leftarrow \textsc{Train}(\mathrm{F}_{\mathrm{MDCS}}, \mathrm{T}_{\mathrm{train}}, \mathrm{NHL})$
      $\mathrm{PM}(n, m) \leftarrow \textsc{Test}(\mathrm{net}, \mathrm{F}_{\mathrm{val}}, \mathrm{T}_{\mathrm{val}})$
    end for
  end for
stage 3: same as MDAS algorithm
end procedure

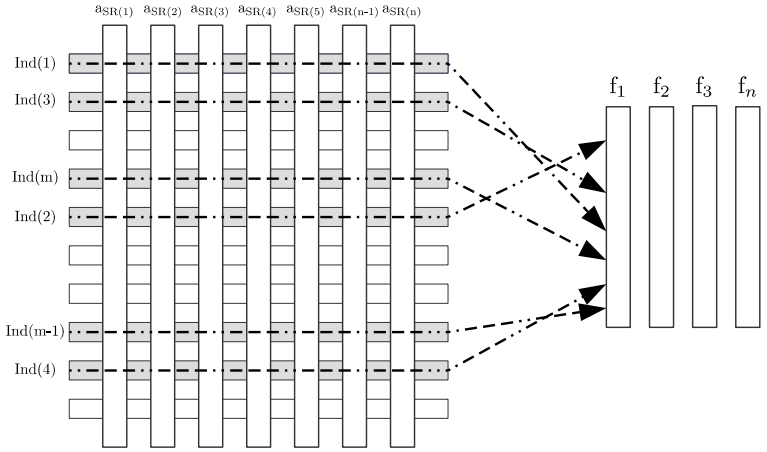

Figure 4: Schematic representation of the coefficient selection process. Here $\mathbf{f}_i$ is a vector whose components are the features extracted from $\mathbf{a}_{\mathrm{SR(i)}}$.

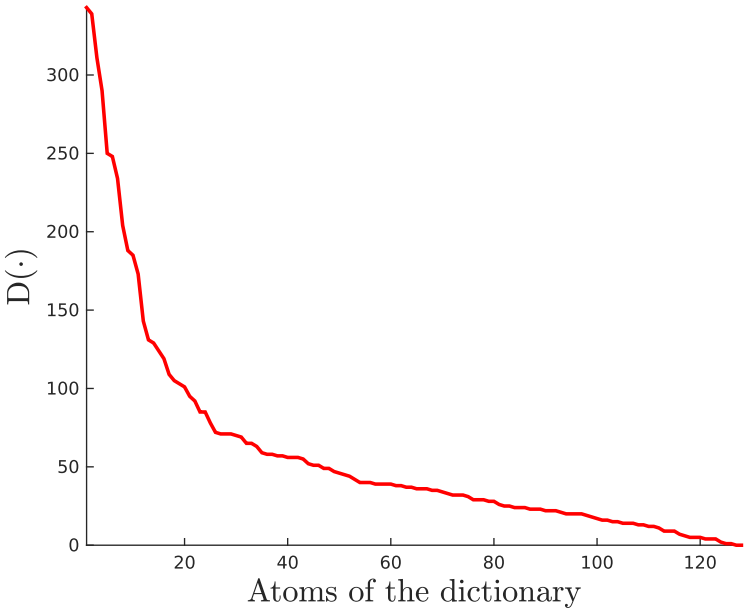

Figure 5: Absolute difference of activation frequency D(·) of the atoms of a dictionary learned with segments of signals belonging to class 1, in decreasing order of magnitude.

cost). The experiments were run on a PC with a 3.5 GHz, 6 cores AMD FX-6300 processor and 8 GB of RAM.

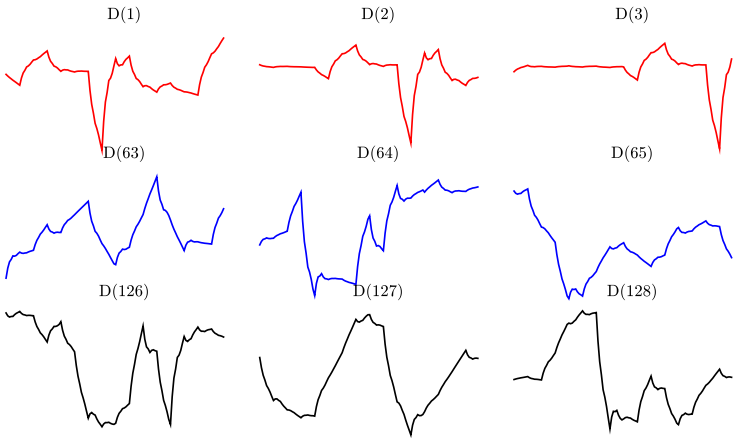

Figure 6: Examples of some atoms of a dictionary learned with segments of signals belonging to class 1 from three different regions of the curve of absolute difference of activation frequency (Figure 5): most discriminative atoms (top), medium discriminative atoms (middle row) and lowest discriminative atoms (bottom row).

3. Results

As mentioned in Subsection 2.1, the complete dataset contains 995 studies, 41 of which were discarded due to incomplete information. Among the remaining 954 studies, a subset of 667 (70%) studies were randomly selected and fixed in order to learn the dictionary and train the MLP neural network. The final test was made using the remaining 287 (30%) studies of the database. The SaO_2 signals were filtered and segmented (see details in Subsection 2.1) into vectors of length 128 (this window size corresponds to 128 seconds of the recording). A matrix $\mathrm{X}_{\mathrm{train}}$ of size 128×455515 was built as $\mathrm{X}_{\mathrm{train}} \doteq [\mathrm{X}^{\mathrm{c1}}_{\mathrm{train}}\ \mathrm{X}^{\mathrm{c2}}_{\mathrm{train}}]$, where the matrices $\mathrm{X}^{\mathrm{c1}}_{\mathrm{train}}$ of size 128×183163 and $\mathrm{X}^{\mathrm{c2}}_{\mathrm{train}}$ of size 128×272352 were constructed considering segments belonging to class 1 and class 2, respectively. Another matrix $\mathrm{X}_{\mathrm{test}}$ was constructed stacking side-by-side all vectors $\mathbf{x}_i$ corresponding to each signal from the testing set.

At the dictionary learning stage, two types of dictionaries were learned using both the $\mathrm{X}^{\mathrm{c1}}_{\mathrm{train}}$ and the $\mathrm{X}^{\mathrm{c2}}_{\mathrm{train}}$ signal matrices. First a complete dictionary Φ_{CD} of size 128×128 was learned using the matrix $\mathrm{X}_{\mathrm{train}}$, without taking into consideration any information about the classes. Second, an overcomplete dictionary Φ_{OD} of size 128×256 was assembled by stacking side-by-side the atoms of two previously learned 128×128 dictionaries Φ^{c1} and Φ^{c2}, which

were learned by using the matrices X^{c1}_{train} and X^{c2}_{train}, respectively. At the dictionary learning stage the atoms were initially taken by random selection from the corresponding signal matrix. The NOCICA method [23] was used for the dictionary learning stage.

The representation coefficients $\mathbf{a}_{SR(i)}$ were obtained by applying the OMP algorithm [25]. The reason for having chosen this greedy algorithm is because it guarantees convergence to the projection of $\mathbf{x}_i$ into the span of the dictionary atoms, in no more than p_0 iterations.

Since our problem involved a big and redundant dataset (big data problem), a variation of the back-propagation algorithm, called mini-batch training procedure, was used to train the MLP neural network. In order to avoid overfitting and estimate the neural network hyper-parameters, a large number of trials with different hyper-parameter values were performed. In what follows, the final choice of the neural network hyper-parameters are described. Batches of 1000 balanced segments were randomly selected from the 455515 available training segments. To avoid overtraining, the number of steps in the scaled conjugate gradient algorithm was set to 4. In addition, to minimize classification bias, the above training scheme was repeated 455 times with re-sampling.

In the proposed algorithms, two parameters need to be empirically determined: the sparsity level p_0 and the threshold of the outputs of the MLP neural network. To determine an adequate sparsity level, several trials were performed. It was found that a percentage value of 12.5 of the signal's space dimension presented the best trade-off between representativity and discriminability of the segments. Hence, sparsity level $p_0 = 16$ was chosen. On the other hand, to establish an optimal threshold of the MLP neural network outputs, different values in the interval $[-0.2, 0.2]$ were tested. A value of zero of the MLP neural network outputs was chosen. Hence an output value greater than 0 was considered as containing an apnea-hypopnea event, and considered to be normal otherwise. Finally the AHI_{est} value was determined as the number of detected events divided by the record length of each study (in seconds).

In Table 1, the columns labeled "F" and "NHL" show the number of inputs (feature vector size) and the number of neurons in the hidden layer of the MLP neural network, respectively. Clearly the application of the MDAS (or MDCS) method produces a significant dimension reduction and therefore, the computing time required for classification is also significant reduced. Thus, for instance, the MDAS-OD method used only 32 features

Table 1: MLP neural network's hyper-parameters. Feature vector size and number of neurons in the hidden layer.

Dictionary	Method	F	NHL
	FULL	256	32
OD	MDAS	32	16
	MDCS	64	32
	FULL	128	32
CD	MDAS	64	32
	MDCS	64	32

(12.5% of the total) compared with the FULL-OD method, which used 256 features.

For analyzing the capability of the proposed classifier in the detection of patients suspected of suffering from OSAH, two measures were introduced. The sensitivity (SE), defined as the ratio of persons with OSAH for whom the trial process is positive, and the specificity (SP), defined as the ratio of patients without OSAH for whom the trial process is negative. Also a receiver operating characteristics (ROC) [26] analysis allows to obtain the following values: true positive (TP), true negative (TN), false positive (FP), false negative (FN), cut-off point (cut-off), and area under the curve (AUC).

The objective of our experiment was to compare the performances of our methods with those of other local approaches used for OSAH detection. In particular, we compared our methods with those introduced by Chiner *et al.* [6] and Vázquez *et al.* [7], and with that presented by Schlotthauer *et al.* [10]. Tables 2, 3, and 4 show the AUC values as well as SE, SP, and accuracy (ACC) measures for AHI diagnostic threshold values of 10 and 15 for the reference.

Table 2 shows the results obtained with the use of sparse representations by means of overcomplete dictionaries. We observed a significant increment in the AUC and SE values obtained with the use of the MDCS (MDCS-OD) method. It can also be seen that the application of the MDAS (MDAS-OD) method does not produce significant changes in the AUC, SE, and SP values. Hence, the best performance of the classifier for the case of overcomplete

Table 2: Performance measures for OSAH detection using an overcomplete dictionary.

Method	AHI_{thr}	AUC	SE(%)	SP(%)	ACC(%)
FULL-OD	10	0.896	**88.37**	75.86	**82.12**
	15	0.923	83.33	**87.32**	85.33
MDAS-OD	10	0.847	86.05	72.41	79.23
	15	0.891	81.02	83.10	82.06
MDCS-OD	10	**0.906**	81.40	**79.31**	80.35
	15	**0.937**	**85.65**	85.92	**85.78**

dictionaries is obtained with the MDCS (MDCS-OD) method.

Table 3 shows the results obtained with the use of sparse representations by means of complete dictionaries. Although the MDAS method produces slight improvements in the AUC, SE, SP, and ACC values as compared with the MDAS-OD method, the results are not the best. In fact, it can be seen that the application of the MDCS method results in the best AUC, SP, and ACC values. A comparison of Tables 2 and 3 allows us to conclude that the application of the MDCS method to sparse representations results in the best option for OSAH detection.

Finally Table 4 presents a comparative summary of the best results (MDCS-OD method) and of those obtained with the other three previously mentioned methods. As observed, our method outperforms all the others. For AHI threshold values of both 10 and 15, our method reaches the maximum AUC values of 0.906 and 0.937, respectively. Also for an AHI threshold value of 15, our method achieves sensitivity and specificity percentages of 85.65% and 85.92%, respectively. The optimal operating point was chosen in order to maximize both the sensitivity and specificity percentages. Figure 7 shows the ROC plots for the four methods presented in Table 4 corresponding to AHI threshold values of 10 (Figure 7a) and 15 (Figure 7b). We also tested the use of a support vector machine (SVM) classifier with a Gaussian kernel function instead of the MLP neural network classifier. No improvements in the results were observed.

Finally, a detailed account of the computational costs for the four methods

Table 3: Performance measures for OSAH detection using a complete dictionary.

Method	AHI_{thr}	AUC	SE(%)	SP(%)	ACC(%)
FULL-CD	10	**0.903**	78.68	**82.76**	80.72
	15	0.930	**85.65**	85.92	85.78
MDAS-CD	10	0.870	73.64	**82.76**	78.20
	15	0.906	**85.65**	85.92	85.78
MDCS-CD	10	0.901	**86.82**	75.86	**81.34**
	15	**0.934**	85.19	**87.32**	**86.25**

at the testing stage is presented in Table 5. It can be observed that although our method needs more than twice of the CPU time required for the other three methods, 2.85 seconds for analyzing the data corresponding to study of ten hours of duration is insignificant, even more so taking into account the improvements in OSAH's detection reached by our method, as it can be observed in Table 4.

4. Discussion

OSAH is a highly prevalent syndrome in the general human population. From a sample of 602 workers, with ages between 30 and 60, Young *et al.* [27] found that 24% of men and 9% of women had an AHI value above 5. Durán *et al.* [28] also found that aging, being male, snoring and obesity are all factors increasing the risk of suffering from OSAH. Given this high prevalence of OSAH, primary attention medicine is determinant in the identification of patients suffering from it and therefore simple and cheap diagnostic tools are highly important. An additional valuable aspect of our work is the fact that we were able to establish a relationship between the final feature vectors and the apnea-hypopnea events. This relationship can be seen in Figure 8. On the upper right of this figure a portion of the wavelet-filtered SaO_2 signal with the marks of apnea-hypopnea events labeled by the medical expert is shown. Immediately below a curve (in green) representing the cumulative absolute activation of the sixteen most discriminative coefficients and the la-

Table 4: Performance measures for OSAH detection using different methods.

Method	AHI_{thr}	AUC	SE(%)	SP(%)	ACC(%)
MDCS-OD	10	**0.906**	**81.40**	79.31	80.35
	15	**0.937**	**85.65**	85.92	**85.78**
Chiner *et al.* [6]	10	0.810	77.87	76.00	76.93
	15	0.795	76.17	78.12	77.15
Vázquez *et al.* [7]	10	0.870	77.47	**84.00**	80.74
	15	0.909	80.84	**87.50**	84.17
Schlotthauer *et al.* [10]	10	0.890	80.63	**84.00**	**82.32**
	15	0.922	84.11	85.94	85.02

Table 5: Computational cost: average CPU time for each study.

Method	Time (seconds)
MDCS-OD	2.85
Chiner *et al.* [6]	0.81
Vázquez *et al.* [7]	1.21
Schlotthauer *et al.* [10]	1.35

bels of apnea-hypopnea events (in red) are presented. The image appearing on the lower right part of Figure 8 shows the absolute value of the sixteen most discriminative coefficients of our method. A high correlation between the tags labeled by the medical experts and the most discriminative coefficients can be clearly observed. On the other hand, on the upper left corner of Figure 8 a segment of 128 seconds of the wavelet-filtered SaO_2 signal with the corresponding marks of apnea-hypopnea events is shown, while immediately below the three most discriminative atoms (ϕ_1, ϕ_8, and ϕ_{13}, respectively) involved in its representation are shown. It can be clearly seen how these three most discriminative atoms assemble together to capture the main features of

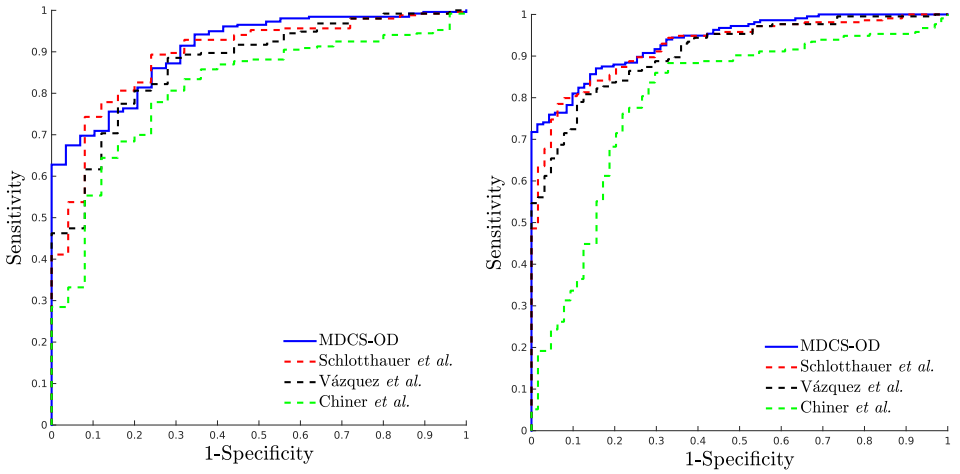

(a) $\mathrm{AHI}_{\mathrm{thr}} = 10$. (b) $\mathrm{AHI}_{\mathrm{thr}} = 15$.

Figure 7: ROC plots for the methods described in Table 4 for two different AHI threshold values.

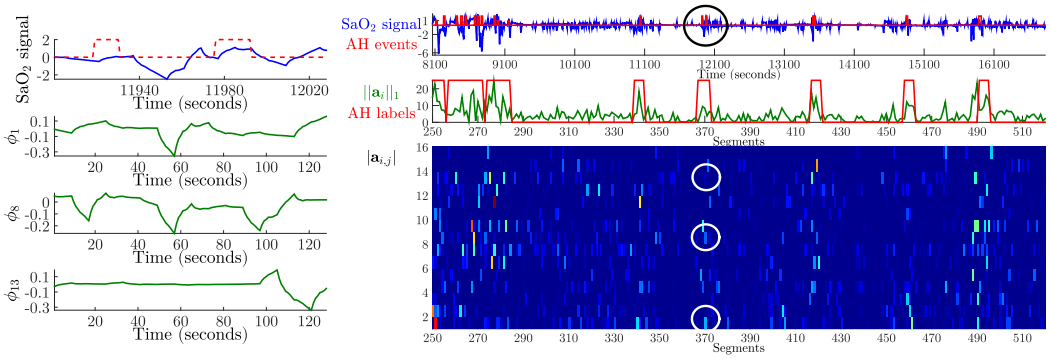

Figure 8: Final feature vectors to apnea-hypopnea events correlation.

the waveform of the filtered SaO_2 signal.

An adequate use of simplified and correctly validated systems would allow, once the cases have been selected, to decentralize the diagnosis of the reference units which are usually saturated. This decentralization would favor the creation of new smaller diagnostic units equipped with oximeters. This decentralization of the diagnostic process will have to be accompanied by appropriate training of the personnel as well as of good coordination with the reference sleep units for a deeper study of the difficult or doubtful cases

[29]. Networks of increasing complexity will have to be created in order to allow immediate consultation with a sleep medicine expert and the possibility of performing, whenever necessary, a polisomnography for the diagnostic and treatment of this real public health problem which is OSAH [29]. The design of diagnostic tools and equipment which could be handled by non-expert personnel for detecting patients with severe OSAH is a priority, since an early identification will allow immediate access to a correct treatment.

Apnea-hypopnea events during sleeping occur as a consequence of a functional-anatomic disturbance of the upper airway producing its collapse. At the end of each apnea-hypopnea event, a desaturation of the hemoglobin usually occurs. This desaturation originates a characteristic pattern in the pulse oximetry record corresponding to intermittent hypoxemia. The intermittent hypoxemia, with hypoxemia-reoxygenation cycles, promotes oxidative stress and angiogenesis, increases the sympathetic activation with increment of blood pressure and systemic and vascular inflammation with endothelial dysfunction which contributes to multi-organic chronic morbility, metabolic dysfunction, cognitive impairment and cancer progression [30].

Due to the intermittent hypoxemia in the cells (hypoxemia-reoxygenation cycles) which induce angiogenesis and tumor growth, a strong correlation between neoplastic diseases and OSAH has been described [31]. On the other hand, a recent study among male mice suggests that the intermittent hypoxia associated with OSAH could induce fertility reduction [32].

In this work we presented two novel methods which allow for the detection of apnea-hypopnea events using only the SaO_2 signals. These methods were successfully applied to signals coming from the polysomnography records in the study database [20, 21]. As it can be observed in Section 3, the application of the FULL, MDAS, and MDCS strategies, both to complete and overcomplete dictionaries, resulted in six different methods. Tables 2 and 3 show the results of each one of the six methods for two different AHI threshold values ($AHI_{thr} = 10$ and $AHI_{thr} = 15$). These threshold values were strategically chosen in order to be able to analyze the performance of each method, independently of the severity of the OSAH (or the AHI value) that one wishes to detect. Although usually an AHI threshold value of 5 is used as the lower limit for detecting mild cases of OSAH, in our case, a reliable ROC analysis for that threshold value could not be made. The main reason for that is the fact our database is highly unbalanced, containing only 16 studies with AHI values below 5. Our random selection of studies resulted in only three of them being considered for testing purposes. A statistically significant

correlation between OSAH's severity and comorbilities, such as hypertension, diabetes, dyslipidemia and metabolic syndrome, has been found in previous works. Although this correlation is found in mild OSAH, it increases consideulrably with the OSAH's degree, reaching its highest value with severe OSAH. Hence if the objective is OSAH treatment and the prevention of the associated comorbilities, an AHI threshold value of 15 is clearly pathological [33]. There is evidence that close to 93% of women and 82% of men with moderate to severe OSAH remain undiagnosed [34]. Since sleep fragmentation, intermittent hypoxemia, increased sympathetic tone and hypertension are main causes of mortality and morbidity, it is highly desirable to have everyone with moderate to severe OSAH appropriately diagnosed. Although the gold standard for diagnosing sleep disorders is the complete PSG, this diagnosing procedure presents many limitations, such as: limited resources, limited number of recording beds, high costs, long waiting lists, and high labor requirements, among others. It is for those reasons that there is a lot of interest in exploring the possibility of using screening devices together with automated algorithms as alternative methods for diagnosing OSAH. Mild cases can be analyzed by standard methods. The ideal screening device should be cheap and easy to be used with minimal risks to the patient.

By considering an $\mathrm{AHI}_{\mathrm{thr}} = 15$, a detailed analysis of Tables 2 and 3 show that, although most methods have good performances, MDCS-OD outperforms all the others. The application of this method results in an area under the ROC curve of 0.937 and sensitivity and specificity percentages of 85.65 and 85.92, respectively. Taking into account that out of the 287 records in the testing database, 216 had an AHI value above 15, and the remaining 71 were below that threshold value, a 85.65% sensitivity indicates that of the 216 cases with AHI values above 15, 185 were appropriately identified while 31 were erroneously detected. On the other hand, an 85.92 specificity indicates that of the 71 cases with AHI values below 15, 61 were appropriately identified while only 10 were erroneously detected. It is timely to point out here that for the 10 cases that the MDCS-OD method yielded an AHI value higher than 15, the registry database indicated an AHI average value of 10.62 with a standard deviation of 3.88. By analyzing each one of these studies in detail, it was observed that most of the respiratory events informed by the medical expert were hypopneas and not all of them were related to SaO_2 desaturations. This fact indicates that the medical experts have not taken into account the AASM criteria.

The MDCS-OD method was compared with those proposed by Chiner *et*

al. [6], Vázquez *et al.* [7], and Schlotthauer *et al.* [10]. These four methods were successfully applied to pulse oximetry signals included in the study database [20, 21]. Table 4 shows a detailed comparison of the performances of such methods. The results clearly show that the MDCS-OD method is a very attractive tool to assist physicians in the detection of patients whose AHI values are above the objective threshold $\mathrm{AHI}_{\mathrm{thr}} = 15$. Thus, the sparse representation of pulse oximetry signals is undoubtedly a promising technique for the design of new methods for OSAH detection.

Since there exist applications where a particular value of sensitivity or specificity is highly desirable, other operation points in the ROC curves (Figure 7) can be chosen. If the primary purpose of the test is "screening", i.e. detection of early disease in large numbers of apparently healthy individuals, then a high sensitivity is generally chosen. With this in mind, if a sensitivity of 98% is chosen in the ROC curves in Figure 7a, our method achieves a specificity of 44.83%, followed by Schlotthauer's *et al.* which reaches 28.00%. For an operating point of 98% sensitivity in the ROC curves in Figure 7b, our method achieves a specificity of 46.48%, followed by Schlotthauer's *et al.* which reaches 34.37%. On the other hand, if the objective test is "diagnostic", i.e. to establish the presence (or absence) of disease, then a high specificity is usually selected. Thus, if a specificity of 100% is chosen in the ROC curves in Figure 7a, our method achieves a sensitivity of 62.79%, followed by Vázquez's *et al.* which reaches 46.25%. For an operating point of 100% sensitivity in the ROC curves in Figure 7b, our method achieves a sensitivity of 71.76%, followed by Vázquez's *et al.* which reaches 54.67%.

There are several technical and physiological limitations associated with pulse oximetry which hinder the acquisition of a "good" signal in some cases. This is so, for instance in the following cases: weak contact between the probe and the finger due to body motions, anemia, use of nail polish, use of artificial nails, skin pigmentation, onychomycosis, cold fingers and low perfusion of vascular bed [35, 36]. Even so, pulse oximetry has shown its effectiveness in clinical practice and therefore an alert and well informed clinical physician must be aware of both its proper use and limitations.

5. Conclusions

It has been shown that the sparse representations of pulse oximetry signals is a tool which allows a very good performance for estimating AHI values above 15. The previous results have been shown that there is a high corre-

lation between the AHI observed by the medical physician via PSG and the AHI_{est} obtained by using sparse representations of pulse oximetry signals. This fact constitutes a strong evidence that such a procedure could be helpful in the detection of individuals suspected of suffering from OSAH, which require a complete PSG study for their correct diagnosis. The MDCS-OD algorithm could be embedded into the oximeter so as to be used by primary attention clinical physicians in the search and detection of patients with moderate OSAH.

Acknowledgment

The authors would like to acknowledge the financial support of Consejo Nacional de Investigaciones Científicas y Técnicas, CONICET, through projects PIP 2014-2016 Nro. 11220130100 216-CO and PIP 2012-2014 Nro. 11420110100284-KA4, of the Air Force Office of Scientific Research, AFOSR /SOARD, through Grant FA9550-14-1-0130 and of the Universidad Nacional del Litoral through projects CAI+D 50120110100519 and CAI+D 5012011010 0525.

6. References

[1] M. J. Sateia, International classification of sleep disorders-third edition: Highlights and modifications, Chest 146 (2014) 1387–1394.

[2] R. Thurnheer, K. E. Bloch, I. Laube, M. Gugger, M. Heitz, Swiss Respiratory Polygraphy Registry, Respiratory polygraphy in sleep apnoea diagnosis. Report of the Swiss respiratory polygraphy registry and systematic review of the literature, Swiss Medical Weekly 137 (2007) 97–102.

[3] E. García-Díaz, E. Quintana-Gallego, A. Ruiz, C. Carmona-Bernal, A. Sánchez-Armengol, G. Botebol-Benhamou, F. Capote, Respiratory polygraphy with actigraphy in the diagnosis of sleep apnea-hypopnea syndrome, Chest 131 (2007) 725–732.

[4] A. Yadollahi, E. Giannouli, Z. Moussavi, Sleep apnea monitoring and diagnosis based on pulse oximetry and tracheal sound signals, Medical & Biological Engineering & Computing 48 (2010) 1087–1097.

[5] L.-W. Hang, H.-L. Wang, J.-H. Chen, J.-C. Hsu, H.-H. Lin, W.-S. Chung, Y.-F. Chen, Validation of overnight oximetry to diagnose patients with moderate to severe obstructive sleep apnea, BMC Pulmonary Medicine 15 (2015) 24.

[6] E. Chiner, J. Signes-Costa, J. M. Arriero, J. Marco, I. Fuentes, A. Sergado, Nocturnal oximetry for the diagnosis of the sleep apnoea hypopnoea syndrome: a method to reduce the number of polysomnographies?, Thorax 54 (1999) 968–971.

[7] J.-C. Vázquez, W. H. Tsai, W. W. Flemons, A. Masuda, R. Brant, E. Hajduk, W. A. Whitelaw, J. E. Remmers, Automated analysis of digital oximetry in the diagnosis of obstructive sleep apnoea, Thorax 55 (2000) 302–307.

[8] D. Alvarez-Estevez, V. Moret-Bonillo, Computer-Assisted Diagnosis of the Sleep Apnea-Hypopnea Syndrome: A Review, Sleep Disorders 2015 (2015).

[9] L. M. Sepulveda-Cano, E. Gil, P. Laguna, G. Castellanos-Dominguez, Selection of nonstationary dynamic features for obstructive sleep apnoea detection in children, EURASIP Journal on Advances in Signal Processing 11 (2011) 1–10.

[10] G. Schlotthauer, L. E. Di Persia, L. D. Larrateguy, D. H. Milone, Screening of obstructive sleep apnea with empirical mode decomposition of pulse oximetry, Medical Engineering & Physics 36 (2014) 1074–1080.

[11] A. R. Hassan, Computer-aided obstructive sleep apnea detection using normal inverse gaussian parameters and adaptive boosting, Biomedical Signal Processing and Control 29 (2016) 22–30.

[12] H. Karamanli, T. Yalcinoz, M. A. Yalcinoz, T. Yalcinoz, A prediction model based on artificial neural networks for the diagnosis of obstructive sleep apnea, Sleep and Breathing 20 (2015) 509–514.

[13] M. S. Lewicki, B. A. Olshausen, Probabilistic framework for the adaptation and comparison of image codes, Journal of the Optical Society of America A 16 (1999) 1587.

[14] M. Aharon, M. Elad, A. Bruckstein, KSVD: An Algorithm for Designing Overcomplete Dictionaries for Sparse Representation, IEEE Transactions on Signal Processing 54 (2006) 4311–4322.

[15] P. König, K. P. Körding, D. J. Klein, Sparse spectrotemporal coding of sounds, EURASIP Journal on Advances in Signal Processing (2003) 659–667.

[16] C. E. Martínez, J. Goddard, D. H. Milone, H. L. Rufiner, Bioinspired sparse spectro-temporal representation of speech for robust classification, Computer Speech and Language 26 (2012) 336–348.

[17] R. Rolón, L. Di Persia, H. L. Rufiner, R. Spies, Most discriminative atom selection for apnea-hypopnea events detection, in: Anales del VI Congreso Latinoamericano de Ingeniería Biomédica (CLAIB 2014), pp. 709–712.

[18] S. Haykin, Neural Networks: A Comprehensive Foundation, Prentice Hall PTR, Upper Saddle River, NJ, USA, 2nd edition, 1998.

[19] F. Lestussi, L. Di Persia, D. Milone, Comparison of on-line wavelet analysis and reconstruction: with application to ECG, 5th International Conference on Bioinformatics and Biomedical Engineering (iCBBE 2011) (2011).

[20] S. F. Quan, B. V. Howard, C. Iber, J. P. Kiley, F. J. Nieto, G. T. O'Connor, D. M. Rapoport, S. Redline, J. Robbins, J. M. Samet, P. W. Wahl, The Sleep Heart Health Study: design, rationale, and methods, Sleep 20 (1997) 1077–1085.

[21] B. K. Lind, J. L. Goodwin, J. G. Hill, T. Ali, S. Redline, S. F. Quan, Recruitment of healthy adults into a study of overnight sleep monitoring in the home: experience of the Sleep Heart Health Study, Sleep & Breathing = Schlaf & Atmung 7 (2003) 13–24.

[22] S. Abdallah, Towards music perception by redundancy reduction and unsupervised learning in probabilistic models, Ph.D. Thesis, Department of Electronic Engineering, King's College London., 2002.

[23] M. S. Lewicki, T. J. Sejnowski, Learning overcomplete representations, Neural Computation 12 (2000) 337–365.

[24] J. Tropp, A. Gilbert, Signal Recovery From Random Measurements Via Orthogonal Matching Pursuit, IEEE Transactions on Information Theory 53 (2007) 4655–4666.

[25] Y. Pati, R. Rezaiifar, P. Krishnaprasad, Orthogonal matching pursuit: recursive function approximation with applications to wavelet decomposition, in: Conference Record of The Twenty-Seventh Asilomar Conference on Signals, Systems and Computers, pp. 40–44.

[26] R. Kumar, A. Indrayan, Receiver operating characteristic (ROC) curve for medical researchers, Indian Pediatrics 48 (2011) 277–287.

[27] T. Young, M. Palta, J. Dempsey, J. Skatrud, S. Weber, S. Badr, The occurrence of sleep-disordered breathing among middle-aged adults, The New England Journal of Medicine 328 (1993) 1230–1235.

[28] J. Durán, S. Esnaola, R. Rubio, A. Iztueta, Obstructive sleep apnea-hypopnea and related clinical features in a population-based sample of subjects aged 30 to 70 yr, American Journal of Respiratory and Critical Care Medicine 163 (2001) 685–689.

[29] Tratamiento médico del SAHS, Archivos de Bronconeumología 41 (2005) 43–50.

[30] N. A. Dewan, F. J. Nieto, V. K. Somers, Intermittent hypoxemia and OSA: implications for comorbidities, Chest 147 (2015) 266–274.

[31] W. Kukwa, E. Migacz, K. Druc, E. Grzesiuk, A. M. Czarnecka, Obstructive sleep apnea and cancer: effects of intermittent hypoxia?, Future Oncology (London, England) 11 (2015) 3285–3298.

[32] M. Torres, R. Laguna-Barraza, M. Dalmases, A. Calle, E. Pericuesta, J. M. Montserrat, D. Navajas, A. Gutierrez-Adan, R. Farré, Male fertility is reduced by chronic intermittent hypoxia mimicking sleep apnea in mice, Sleep 37 (2014) 1757–1765.

[33] M. Fusetti, A. B. Fioretti, M. Valenti, F. Masedu, M. Lauriello, M. Pagliarella, Cardiovascular and metabolic comorbidities in patients with obstructive sleep apnoea syndrome, Acta Otorhinolaryngologica Italica 32 (2012) 320–325.

[34] T. Young, L. Evans, L. Finn, M. Palta, Estimation of the clinically diagnosed proportion of sleep apnea syndrome in middle-aged men and women, Sleep 20 (1997) 705–706.

[35] R.-P. Eduardo Martín, Factores que afectan la oximetría de pulso, Revista Mexicana de Anestesiología 29 (2006) S193–S198.

[36] M. George, S. Ronald E., Limitations of Pulse Oximetry, Anesthesia Progress 39 (1992) 194–196.

677 **AppendixA. Dictionary updating rule.**

Proof.

$$\begin{aligned}\Delta\Phi &= \eta\Lambda_\epsilon\mathbb{E}[(\mathbf{x}-\Phi\mathbf{a})\mathbf{a}^T] \\ &= \eta\Lambda_\epsilon\mathbb{E}[(\mathbf{x}\mathbf{a}^T-\Phi\mathbf{a}\mathbf{a}^T)] \\ &= \eta\Lambda_\epsilon(\mathbf{x}\mathbb{E}[\mathbf{a}^T]-\Phi\mathbb{E}[\mathbf{a}\mathbf{a}^T]).\end{aligned}$$

678 But

$$\mathbb{E}[\mathbf{a}^T] = \mathbf{a}_{\text{MAP}}^T,$$

679 and

$$\begin{aligned}\text{cov}(\mathbf{a}) &= \mathbb{E}[(\mathbf{a}-\mathbf{a}_{\text{MAP}})(\mathbf{a}^T-\mathbf{a}_{\text{MAP}}^T)] \\ &= \mathbb{E}[\mathbf{a}\mathbf{a}^T-\mathbf{a}\mathbf{a}_{\text{MAP}}^T-\mathbf{a}_{\text{MAP}}\mathbf{a}^T+\mathbf{a}_{\text{MAP}}\mathbf{a}_{\text{MAP}}^T] \\ &= \mathbb{E}[\mathbf{a}\mathbf{a}^T]-\mathbb{E}[\mathbf{a}\mathbf{a}_{\text{MAP}}^T]-\mathbb{E}[\mathbf{a}_{\text{MAP}}\mathbf{a}^T]+\mathbb{E}[\mathbf{a}_{\text{MAP}}\mathbf{a}_{\text{MAP}}^T] \\ &= \mathbb{E}[\mathbf{a}\mathbf{a}^T]-\mathbb{E}[\mathbf{a}]\mathbf{a}_{\text{MAP}}^T-\mathbf{a}_{\text{MAP}}\mathbb{E}[\mathbf{a}^T]+\mathbf{a}_{\text{MAP}}\mathbf{a}_{\text{MAP}}^T \\ &= \mathbb{E}[\mathbf{a}\mathbf{a}^T]-\mathbf{a}_{\text{MAP}}\mathbf{a}_{\text{MAP}}^T-\mathbf{a}_{\text{MAP}}\mathbf{a}_{\text{MAP}}^T+\mathbf{a}_{\text{MAP}}\mathbf{a}_{\text{MAP}}^T \\ &= \mathbb{E}[\mathbf{a}\mathbf{a}^T]-\mathbf{a}_{\text{MAP}}\mathbf{a}_{\text{MAP}}^T \\ \mathbb{E}[\mathbf{a}\mathbf{a}^T] &= \text{cov}(\mathbf{a})+\mathbf{a}_{\text{MAP}}\mathbf{a}_{\text{MAP}}^T.\end{aligned}$$

680 Hence,

$$\begin{aligned}\Delta\Phi &= \eta\Lambda_\epsilon(\mathbf{x}\mathbf{a}_{\text{MAP}}^T-\Phi(\text{cov}(\mathbf{a})+\mathbf{a}_{\text{MAP}}\mathbf{a}_{\text{MAP}}^T) \\ &= \eta\Lambda_\epsilon(\mathbf{x}\mathbf{a}_{\text{MAP}}^T-\Phi(H^{-1}+\mathbf{a}_{\text{MAP}}\mathbf{a}_{\text{MAP}}^T) \\ &= \eta\Lambda_\epsilon(\mathbf{x}\mathbf{a}_{\text{MAP}}^T-\Phi H^{-1}-\Phi\mathbf{a}_{\text{MAP}}\mathbf{a}_{\text{MAP}}^T) \\ &= \eta\Lambda_\epsilon((\mathbf{x}-\Phi\mathbf{a}_{\text{MAP}})\mathbf{a}_{\text{MAP}}^T-\Phi H^{-1}).\end{aligned}$$

681 □